Am J Physiol Renal Physiol
278: F540–F553, 2000.

Urothelial pathophysiological changes in feline interstitial cystitis: a human model

JOHN P. LAVELLE,[1] SUSAN A. MEYERS,[2] W. GIOVANI RUIZ,[2]
C. A. TONY BUFFINGTON,[3] MARK L. ZEIDEL,[2] AND GERARD APODACA[2]
[1]*Department of Urology, and* [2]*Laboratory of Epithelial Cell Biology, Renal-Electrolyte Division, Department of Medicine, University of Pittsburgh Medical Center, Pittsburgh, Pennsylvania 15213; and* [3]*Ohio State University Veterinary Hospital, Columbus, Ohio 43210-1089*

Lavelle, John P., Susan A. Meyers, W. Giovani Ruiz, C. A. Tony Buffington, Mark L. Zeidel, and Gerard Apodaca. Urothelial pathophysiological changes in feline interstitial cystitis: a human model. *Am J Physiol Renal Physiol* 278: F540–F553, 2000.—Unique barrier properties of the urothelial surface membrane permit urine storage. Interstitial cystitis causes disabling dysuria, and frequency. Similarly, feline interstitial cystitis (FIC) occurs in cats. These studies define the permeability and structural properties of normal and FIC urothelium. To determine the effects of bladder filling, groups were studied before and after hydrodistention. Normal urothelium with or without hydrodistention exhibited high transepithelial resistances (TER) and low water and urea permeabilities, resembling other species. Fluorescence confocal microscopy revealed localization of the marker AE-31 to the apical surface of all umbrella cells in normal urothelium, with the tight junction protein ZO-1 localized to tight junctions. Scanning and transmission electron microscopy revealed uniform distribution of luminal cells with characteristic apical membrane and tight junction morphology. Urothelium in FIC animals displayed reduced TER and increased water and urea permeability following hydrodistention. Structural studies in FIC revealed denuded urothelium, with appearance of AE-31 in underlying epithelial cells. The results demonstrate severe epithelial damage and dysfunction in FIC and suggest novel approaches toward examining the etiology and therapy of IC.

epithelial permeability; urinary bladder; pathophysiology; ultrastructure

BLADDER EPITHELIAL CELLS maintain large chemical and electrical gradients between the urine and the blood, despite the fact that many urine constituents such as water, urea, and ammonia are highly permeable across nearly all biological membranes (16, 21, 22). The barrier consists of the apical membrane and tight junctions of the uppermost urothelial layer, the umbrella cells (17, 23, 25, 32). These large multinucleated (20) cells are characterized by apical membranes containing a specific set of proteins, in high concentrations, called uroplakins, as well as highly developed tight junctions. The uroplakins form plaques of protein found only in the outer luminal leaflet of the apical membrane. Between the plaques of uroplakins are membrane hinge-like regions that form ridges on the luminal surface of the normal bladder epithelium. It is hypothesized that when the bladder fills, these hinge regions flatten out, and large numbers of apical submembrane vesicles, containing uroplakins, fuse with the apical membrane. This dramatically expands the surface area with the umbrella cells becoming flatter. The excess membrane undergoes endocytosis when the bladder empties (9, 18, 19, 29, 41), and the surface area decreases, reforming the submembrane vesicles. Deep to the umbrella cells are intermediate and basal cells that form the rest of the transitional bladder epithelium (urothelium).

Interstitial cystitis (IC) is a chronic debilitating syndrome characterized by all of the symptoms of acute bacterial cystitis, including frequency, urgency, nocturia, and bladder/pelvic pain, without any abnormal findings on conventional urine culture and cytology studies. Despite the fact that 300,000 to 500,000 people, mostly women, suffer from this condition in the United States (13), little is known about its pathogenesis. Not surprisingly, treatment has been empiric and only marginally effective. Because the symptoms suggest a chronic irritation of the bladder wall, attention has focused on the possibility that IC is caused by failure of the bladder epithelial permeability barrier (7, 12, 24, 36, 45). Semiquantitative measurements of the ability of human bladders to retain radiolabeled urea provided evidence that in IC patients. urea may leak across the bladder wall (37). Moreover, recent ultrastructural studies of biopsies taken from IC patients during hydrodistention of the bladder (during cystoscopy) demonstrate clearcut evidence of urothelial injury (10, 12, 13).

Research into the causes and treatment of IC has been hampered by the lack of an adequate animal model of the disease. Cats, llamas, and dogs develop a similar condition. Feline interstitial cystitis (FIC) is characterized by symptoms of cystitis, without any evidence of bacterial cystitis, in cats (8). On gross pathology, the findings are similar to those of human IC and include urothelial ulceration with mural inflammation and fibrosis. Unlike IC, which occurs predominantly in females, FIC occurs equally in both sexes (6, 8).

The costs of publication of this article were defrayed in part by the payment of page charges. The article must therefore be hereby marked "*advertisement*" in accordance with 18 U.S.C. Section 1734 solely to indicate this fact.

 0363-6127/00 $5.00 Copyright © 2000 the American Physiological Society

The present studies were designed to examine the functional and structural effects on umbrella cells of this form of noninfectious cystitis in cats. We examined the barrier function of the bladders of normal cats and animals with FIC and performed detailed ultrastructural and immunofluorescence microscopy studies. The results demonstrate failure of the urothelial permeability barrier and damage to the urothelium in cats with FIC.

MATERIALS AND METHODS

Materials. Unless specified otherwise, all chemicals were obtained from Sigma (St. Louis, MO) and were of reagent grade. The [^{14}C]urea [specific activity 2–10 mCi/mmol (i.e., 74–370 MBq/mmol)], and $^{3}H_2O$ [specific activity 1 mCi/g (i.e., 37.0 MBq/g)] were obtained from Dupont New England Nuclear (Wilmington, DE).

All animal studies were carried out in strict compliance with, and with the approval of, the University of Pittsburgh Animal Care and Use Committee; animals were maintained and euthanized according to the standards set forth in the American Physiological Society's Guiding Principles in the Care and Use of Animals. The media used for dissection of the tissue and in the Ussing chambers was a modified Ringer solution previously described (32). Cats, both normal and with confirmed FIC, were obtained from a colony maintained at the Ohio State University College of Veterinary Medicine. All cats with FIC had clinical (painful frequency) and cystoscopic confirmation (development of glomerulations or ulcers with distention of the bladder) of the diagnosis prior to the study.

The cats (male and female, 3–5 kg) were divided into normal and FIC groups, and some of each type were subjected to hydrodistention under general anesthesia before excision of the bladder and euthanasia. Hydrodistension was performed to confirm the diagnosis of interstitial cystitis. A hallmark of this condition is the formation of glomerulations in all regions of the bladder. These are small areas of mucosal hemorrhage, found when the bladder is stressed by distention to 80 cmH_2O pressure with fluid. Occasional glomerulations occur in normal bladders when subjected to the same stress, but not in all quadrants of the bladder, which is a hallmark of IC. Hydrodistention also provides a standard stress to the urothelium.

Anesthesia was induced by inhalation of 5% halothane in oxygen and maintained with ketamine (20 mg/kg im) and xylazine (1 mg/kg im) for the duration of the procedure. All cats had the urethra cannulated with a 3.5-French tom cat catheter (Sherwood Medical, St. Louis, MO). Hydrodistention (if performed) was performed through the urethral catheter, with 0.9% NaCl solution (NS) to 80 cmH_2O for 5 min prior to excision of the bladder. The abdomen was then opened with a lower midline incision. The urinary bladder was identified, and the vascular pedicles were clamped and divided. The urethra was identified and divided, thus allowing excision of the bladder. At the end, the cats were euthanized with pentobarbital sodium (100 mg/kg iv).

Studies of barrier epithelial function. Immediately after excision, the bladders were opened from bladder neck to the dome and placed in Ringer solution. They were then divided in two, and each half was, in turn, placed face down on a rack to stretch the epithelium as previously described (23, 27, 32). The muscle was dissected off the epithelium taking care not to damage or touch the luminal surface of the epithelium. After the muscle was completely removed, the epithelium (2-cm^2 surface area) was mounted on rings between two halves of an Ussing chamber (hemichambers). The epithelia were allowed to stabilize for ~1 h before the addition of isotope and measurement of permeability. The chambers were kept at 37°C and stirred constantly with magnetic stir bars as described (27, 32). Transepithelial resistance (TER) and short-circuit current were recorded throughout the experiments, using a four-electrode current/voltage clamp (Warner Instruments, Hamden, CT) (27).

Permeability measurements. These were performed as described (23, 27, 32). [^{14}C]urea (0.25 μCi/ml) and $^{3}H_2O$ (1 μCi/ml) were added to the apical (luminal) side of the epithelium, and both hemichambers were then sampled at 15-min intervals throughout the experiment. After 1 h of baseline measurements, nystatin (185 μM), a nondiscriminate pore former in the apical membrane, was added to the apical side to increase permeability. To determine the contribution of unstirred layers (the other parts of the cell and areas of unstirred solution next to the exterior membranes) to the measured permeabilities, the apical membrane was disrupted by the addition of 100 μl of Triton X-100, 1 h after nystatin had been added. In all experiments, addition of nystatin and Triton X-100 abolished TER. Corrections were made for removing the sample volume by the addition of replacement fresh Ringer solution, and the calculated fluxes were corrected for these modest dilutional effects.

The calculation of permeability was performed as previously described (23, 32). The surface area determination is based on capacitance measurements made during the baseline period. The method of the capacitance measurement is as described (26, 27).

Antibodies and other reagents. Rat monoclonal antibody to ZO-1, a protein associated with tight junctions, was obtained from Chemicon (Temecula, CA) and used at 1:100 dilution. Supernatant from the mouse monoclonal antibody AE-31 hybridoma was kindly provided by Dr. T. T. Sun (New York University) and used at 1:20 dilution. This antibody recognizes a urothelial-specific 27-kDa antigen (42) that is distinct from the recently cloned 27-kDa uroplakin Ia and 28-kDa uroplakin Ib (42). Immunofluorescent and electron microscopic localization showed that AE-31 antigen is associated with cytoplasmic vesicles and the asymmetric unit membrane plaques of the urothelial apical surface (43). However, like the uroplakins, AE-31 is concentrated only on the apical membrane of the umbrella cells and has not been localized in any other tissue or cell type (44). FITC- or Texas Red-conjugated goat anti-rat IgG or goat anti-mouse IgG were obtained from Jackson ImmunoResearch Laboratories (West Grove, PA) and used at 10–20 μg/ml. The anti-rat and anti-mouse antibodies have minimal cross-reactivity with one another.

Fixation and fluorescent labeling of urothelial cells. Freshly isolated, nonhydrodistended, cat bladders were cut open and mounted on racks, and the muscle was carefully dissected from the overlying connective tissue and mucosa as described above. The tissue was then fixed with paraformaldehyde using a pH-shift protocol (1, 5).

The fixed tissue was incubated with the appropriate primary antibodies, diluted in PBS-fish skin gelatin (FSG)-saponin, for 45 min at 37°C in a humid chamber, and then washed three times, for 5 min each time, with PBS-FSG-saponin. Subsequently, the tissue was incubated 45 min at 37°C with the appropriate combination of fluorescently labeled secondary antibodies and propidium iodide (2 μg/ml) diluted in PBS-FSG-saponin. The tissue was washed three times, for 3 min each time, with PBS-FSG-saponin followed by a 5-min wash in PBS, pH 8.0, alone. The tissue was postfixed in 4% paraformaldehyde dissolved in 100 mM sodium cacodylate, pH 7.4, for 15 min at room temperature,

washed twice with PBS, and mounted in *p*-phenylene diamine as described previously (33).

Scanning laser confocal analysis of fluorescently labeled bladder epithelium. The samples were analyzed using a krypton-argon laser coupled to a Molecular Dynamics (Mountain View, CA) Multiprobe 2001 confocal, attached to a Diaphot microscope (Nikon, Melville, NY) with a Plan Apo ×40 1.3 NA or Plan Apo ×60 1.4 NA objective lens (Nikon). The samples were scanned using the appropriate filter combinations. Collection parameters were as follows: laser output = 25–50 mW, PMT-1 and PMT-2 set to 750 mV, laser attenuation at 3%, 50-μm slit. The images (512 × 512 pixels) were acquired using ImageSpace software and converted to tag information file format (TIFF), and the contrast levels of the images were adjusted in the Photoshop program (Adobe, Mountain View, CA) on a Power PC Macintosh 9500 (Apple, Cupertino, CA). Every attempt was made to collect and process images in an identical manner. The contrast-corrected images were imported into Freehand (Macromedia, San Francisco, CA) and printed from a Kodak 8650PS dye sublimation printer.

Transmission electron microscopy of bladder epithelium. Freshly isolated cat bladders from normal cats or those with FIC were cut open and mounted on racks, and the muscle was carefully dissected from the overlying connective tissue and mucosa as described above. The dissected epithelium was fixed in 2.0% (vol/vol) glutaraldehyde, 2.0% (wt/vol) paraformaldehyde in 200 mM sodium cacodylate, pH 7.4, 1 mM $CaCl_2$, and 0.5 mM $MgCl_2$ for 90 min at room temperature. The tissue was washed three times over a 15-min period with 200 mM sodium cacodylate buffer, pH 7.4, cut into small blocks, and treated with 1.5% OsO_4 (wt/vol), 100 mM sodium cacodylate, pH 7.4, for 60 min at room temperature. After several rinses with H_2O, the samples were en bloc stained overnight with 0.5% (wt/vol) uranyl acetate in H_2O. Samples were dehydrated in a graded series of ethanol, embedded in the epoxy resin LX-112 (Ladd, Burlington, VT), and sectioned with a diamond knife (Diatome, Fort Washington, PA). Sections, silver to pale gold in color, were mounted on butvar-coated nickel grids, contrasted with uranyl acetate and lead citrate, and viewed at 80 kV in a JEOL model 100 CX electron microscope.

Scanning electron microscopy of bladder epithelium. Dissected bladder epithelium (with or without hydrodistention) was fixed in 2.0% (vol/vol) glutaraldehyde, 2.0% (wt/vol) paraformaldehyde in 200 mM sodium cacodylate, pH 7.4, 1 mM $CaCl_2$, and 0.5 mM $MgCl_2$ for 90 min at room temperature. The samples were cut into 5 mm × 5 mm blocks and washed three times over 45 min in PBS. The samples were then dehydrated for 15 min each in the following graded series of ethanol: 30% (vol/vol in PBS), 50% (vol/vol in PBS), 70% (vol/vol in PBS), and 95% (vol/vol in water). Then the samples were incubated three times over a 45-min period in absolute ethanol. The dehydrated samples were critical point dried, sputter coated with gold-palladium, and viewed in a JEOL model JSM T300 scanning electron microscope at 20 kV. Images were captured on Kodak type 52 film, scanned on an Agfa (Woburn, MA) Arcus II scanner, contrast corrected in Photoshop 4.0 (Adobe, San Jose, CA), and assembled and output in the same manner as the confocal microscopy images described above.

Statistical analysis. Results are expressed as means ± SE. Statistical significance is taken at less than 5% probability ($P < 0.05$). A multivariate analysis was performed to determine the overall degree of variability. The subsequent analysis of individual parameters was performed using the Tukey or Dunn method of non-parametric analysis. The analysis was performed with the SPSS statistical package.

RESULTS

TER and permeabilities of normal cat urothelium. TER for normal cat urothelium averaged 3.3 ± 0.56 $k\Omega \cdot cm^2$ ($n = 6$) without prior hydrodistention, and significantly increased to 10.6 ± 1.1 $k\Omega \cdot cm^2$ ($n = 6$, $F = 37.032$, $P < 0.001$) following hydrodistention (Fig. 1). Hydrodistention applies a standard stress to the urothelium, which has been used empirically by urologists to aid in the diagnosis of IC. This stress causes the formation of glomerulations in the urothelium that are more marked in inflammatory conditions of the bladder. Exposure of the epithelia to nystatin, a cation pore former, and Triton X-100, a detergent that destroys the apical membrane, markedly reduced TER (values less than 200 $\Omega \cdot cm^2$), indicating disruption of the epithelial barrier. Figure 2 shows the effects of addition of nystatin followed by Triton X-100 on actual observed water permeability values in normal nondistended bladders ($n = 6$). Using the permeability values obtained following Triton X-100, the unstirred layer value, allowed calculation of the diffusive permeability of the apical membrane of the urothelium, $P_{D(AM)}$ (32). For water, these values in normal cat epithelium averaged 4.01 ± 0.81 × 10^{-5} cm/s ($n = 6$) without prior hydrodistention, and 3.6 ± 0.4 × 10^{-5} cm/s ($n = 6$, not significant) following hydrodistention (Fig. 3). Urea $P_{D(AM)}$ values for these same groups ($n = 6$) averaged 1.5 ± 0.3 × 10^{-6} cm/s and 1.1 ± 0.52 × 10^{-6} cm/s ($n = 3$), respectively (Fig. 4). In summary, there was a significant increase in the resistance on hydrodistention in normal bladders. The permeability to water and urea was unchanged in normal bladders regardless of being distended. As shown in Table 1, these values were similar to resistance and permeability values that we have obtained in several other species. These permeabil-

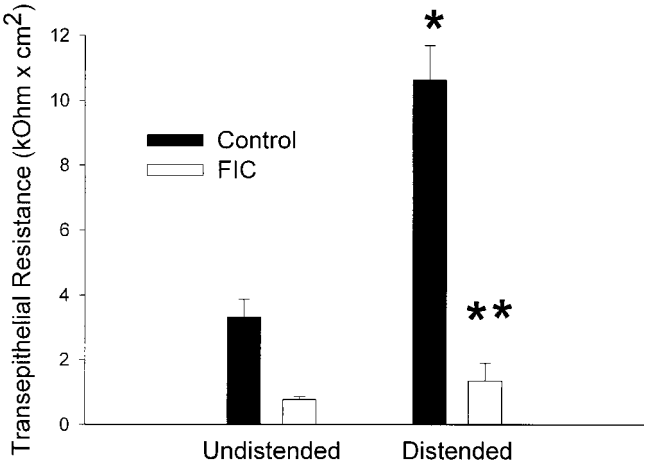

Fig. 1. Effect of feline interstitial cystitis (FIC) on transepithelial resistance (TER) in undistended and hydrodistended bladders. ** Statistically significant difference ($P < 0.01$) between distended normal ($n = 6$) and FIC bladders. In undistended bladders, normal resistance ($n = 6$) did not statistically differ from FIC resistance (*$P = 0.07$). However, TER significantly increased between undistended and distended normal bladders ($P < 0.01$)

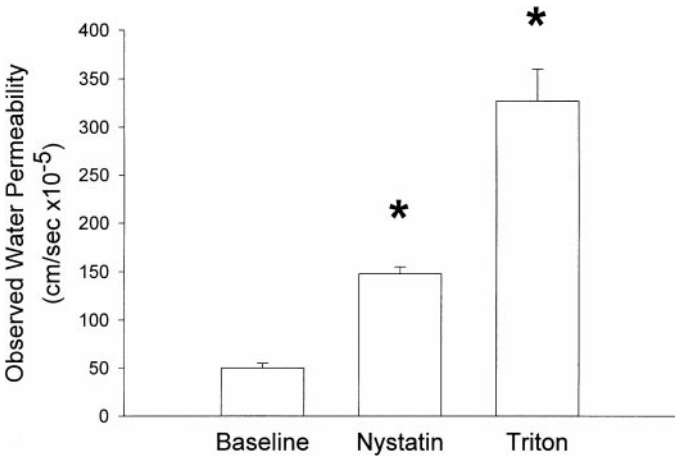

Fig. 2. Effect of nystatin and Triton X-100 on observed water permeability in normal undistended cat bladders. Following a baseline period, nystatin and then Triton X-100 were added to apical surface. *Significant increases in water permeability over baseline following addition of nystatin and Triton X-100 ($n = 6$, $P < 0.05$).

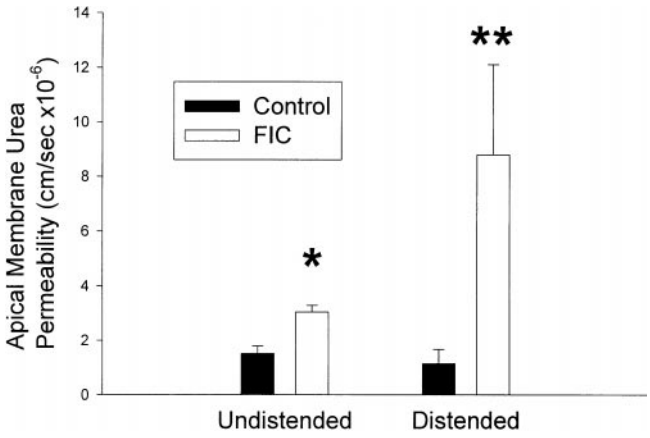

Fig. 4. Effect of FIC on apical membrane urea permeabilities of undistended and hydrodistended bladders. All permeability values were corrected for unstirred layer effects. *Statistical significance between normal and FIC cats in undistended state ($P < 0.05$). **Statistical significance between normal and FIC cats in distended state ($P < 0.01$).

ity values are exceptionally low and confirm that the bladders in many mammalian species exhibit extremely tight barrier properties.

Effect of FIC on barrier function prior to and following hydrodistention. Figures 1, 3, and 4 compare the TERs and $P_{D(AM)}$ values for water and urea of bladders from normal or FIC animals, with and without hydrodistention. In undistended bladders, TER (Fig. 1) in FIC animals was significantly decreased [normal 3.3 ± 0.54 ($n = 6$) vs. FIC 0.77 ± 0.1 kΩ·cm^2 ($n = 3$)]. Water permeability (Fig. 3) was not altered by FIC in undistended bladders [normal 4.0 ± 0.8 × 10^{-5} ($n = 6$) vs. FIC 4.6 ± 0.5 × 10^{-5} cm/s ($n = 3$)]. Urea permeability (Fig. 4) [normal 1.5 ± 0.3 × 10^{-6} ($n = 6$) vs. FIC 3.0 ± 0.2 × 10^{-6} cm/s ($n = 3$)] doubled ($P = 0.018$) in the cats with FIC with undistended bladders.

In cats with FIC, hydrodistention led to marked variability in TER [normal hydrodistended TER = 10.6 ± 1 kΩ·cm^2 ($n = 6$) vs. FIC hydrodistended 1.3 ± 0.6 kΩ·cm^2 ($n = 6$) vs. FIC undistended 0.77 ± 0.1 kΩ·cm^2 ($n = 3$)]. Despite the variation, the resistance did not significantly increase in FIC cats with hydrodistention. There was a significant difference between the TER of the normal and FIC hydrodistended bladders ($P < 0.001$) which was more pronounced than that of the undistended bladders (Fig. 1). Water permeability in hydrodistended bladders from FIC affected cats doubled, with a significant increase compared with hydrodistended normal cat bladders (Fig. 3) [normal 3.6 ± 0.9 × 10^{-5} ($n = 6$) vs. FIC 8.7 ± 1.3 × 10^{-5} cm/s ($n = 6$) ($P < 0.001$)]. Urea permeability associated with FIC (Fig. 4) also significantly increased after hydrodistention [normal 1.14 ± 0.52 × 10^{-6} ($n = 5$) vs. FIC 8.8 ± 3.3 × 10^{-6} cm/s ($n = 5$) ($P = 0.016$)].

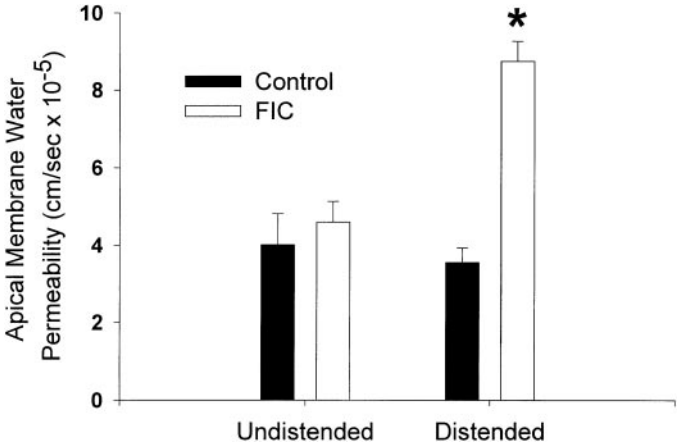

Fig. 3. Effect of FIC on apical membrane water permeabilities of undistended and distended bladders. All permeability values have been corrected for unstirred layer effects. *Statistical significance between normal and FIC water permeability in distended state ($P < 0.01$).

Figure 5 compares TERs to urea permeabilities for all studies performed. It is apparent that once resistance reaches a lower threshold value, of approximately 1 kΩ·cm^2, urea permeability increases markedly. At high TER, the permeability of urea is low but the relationship between high TER and low permeability is complex and not directly proportional. A similar finding was found in the relationship between water permeability and TER in the rabbit bladder (32).

Laser scanning confocal fluorescence microscopy. We have examined the distribution of two proteins that are associated with the umbrella cell layer: ZO-1 and

Table 1. *Comparison of TER and apical membrane water and urea permeabilities between cat, guinea pig, rat, and rabbit*

Species	TER, kΩ·cm^2	$P_{D(AM)}$, cm/s	
		Water (×10^{-5})	Urea (×10^{-6})
Cat	3.3 ± 0.56	4.01 ± 0.81	1.5 ± 0.3
Guinea pig	2.38 ± 0.29	5.74 ± 0.71	1.67 ± 0.08
Rat	1.25 ± 0.15	4.64 ± 0.78	1.69 ± 0.45
Rabbit	3.21 ± 0.80	5.15 ± 0.43	4.51 ± 0.67

Values are means ± SE. TER, transepithelial resistance; $P_{D(AM)}$, apical membrane permeability.

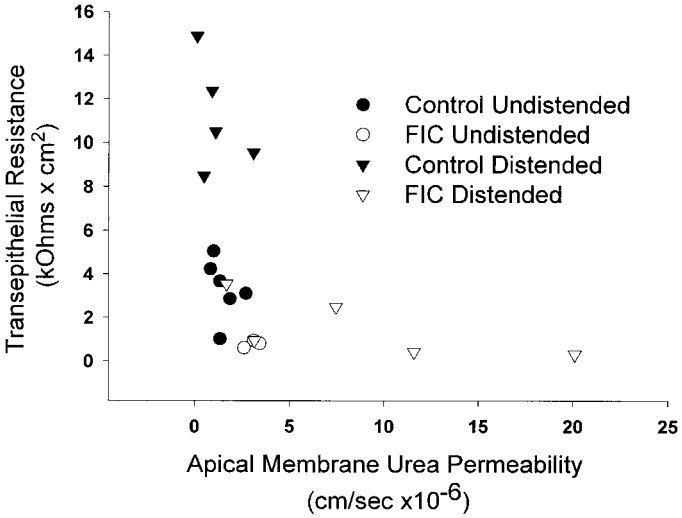

Fig. 5. Relationship between apical membrane urea permeability (abscissa) and TER (ordinate) for all bladders studied.

AE-31. ZO-1 is a cytoplasmic constituent of the tight junction complex, whereas AE-31 is a monoclonal antibody that recognizes a 27-kDa urothelial-specific differentiation marker of the umbrella cell (44). The AE-31 antigen is found mainly on the apical membrane of umbrella cells and in the subapical vesicles. To examine the three dimensional distribution of these antigens, we have used scanning laser confocal microscopy, which allowed us to simultaneously determine the distribution of ZO-1 and the AE-31 antigen. The nuclei of the cells were stained with propidium iodide, and the emission of this dye collected in the same channel as that of ZO-1.

A series of low-magnification optical sections from normal bladders are shown in Fig. 6, *A–H*, and higher magnification images are shown in Fig. 6, *I–P*. Confocal microscopy of normal urothelium from a representative nondistended feline bladder (Fig. 6) revealed consistent, polygonal lattice-like labeling of the upper surface umbrella cells with ZO-1, indicating its distribution in the tight junctions. Nuclei of umbrella cells and underlying urothelial cells are also visible. ZO-1 was not observed in the lower layers (compare Fig. 6*A* to 6*G* and Fig. 6*I* to 6*O*). Similar results were observed in three separate animals. When AE-31 is examined in the same sections, it exhibited surface labeling in the umbrella cells only; underlying intermediate and basal urothelial cells remained unlabeled (see Fig. 6, *H* and *P*).

A series of representative low-magnification optical sections from FIC bladders are shown in Fig. 7, *A–H*, and higher magnification images are shown in Fig. 7, *I–P*. In contrast to the regular staining observed in normal cats, examination of the three nondistended bladders from cats with FIC revealed large areas of denuded umbrella cells, which left areas of underlying urothelial cells exposed to the surface (Fig. 7, *A–H*). ZO-1 was found in its characteristic distribution in the umbrella cells. The intensity of labeling for ZO-1 of the surface urothelial cells that remained appeared to be similar to that of umbrella cells from normal bladders. There was little of this antigen detected in the region of the smaller cells, suggesting that tight junction formation was absent or diminished in these regions of the urothelium. At higher magnification, it was apparent that the smaller cells were in a lower focal plane than the adjacent umbrella cells (Fig. 7, *I* and *J*) and were most likely intermediate in the process of regenerating the umbrella cell layer (see Fig. 10*B*). There was a limited amount of ZO-1 staining associated with the intermediate cells adjacent to the umbrella cells. The underlying urothelial cells did not express detectable ZO-1.

The smaller underlying urothelial cells that were exposed expressed abundant levels of the AE-31 antigen (Fig. 7*B*), which localized in a perinuclear, rather than an apical membrane distribution. AE-31 antigen expression in the intermediate cell layer also was greater than that of the surrounding umbrella cells. AE-31 labeling was not detected in urothelium that was not exposed, suggesting that denuding of umbrella cells and exposure of underlying urothelium was associated with expression of this apical umbrella cell antigen. There was no change in the surface labeling of intact umbrella cells for AE-31. The significance of the perinuclear staining may represent newly synthesized AE-31 associated proteins, as the intermediate cells mature to umbrella cells, in the Golgi or endoplasmic reticulum. In the umbrella cell these structures are organized around the nucleus.

Scanning electron microscopy. Scanning and transmission electron microscopy were performed on two normal and two FIC animals. Scanning electron micrographs of normal cat bladder revealed a highly regular layer of umbrella cells overlying the entire surface of the nonhydrodistended bladder (see Fig. 8*A* and higher magnification Fig. 8*B*). Each cell was surrounded by a junctional complex, and the surface of each cell contained numerous microscopic folds with a rigid, angular appearance (see *inset* of Fig. 8*B*). Occasionally, one or two umbrella cells were missing when large areas were surveyed. Undistended bladders from cats with FIC exhibited striking changes in epithelial structure when compared with normal bladders. Scanning electron microscopy revealed patches of normal looking urothelium and multiple patches in which umbrella cells were missing, exposing the underlying urothelial cells. As shown in Fig. 9*A*, these patches were often larger than the areas of 5–20 umbrella cells.

There were regions between cells in which portions of adjacent umbrella cells appeared to be detached (see arrows in Fig. 9*A*), suggesting a loss of cell-cell adhesion. Many umbrella cells retained their angular apical plasma membrane; however, some appeared to have a smoother cell surface, indicating a loss of the characteristic plaque/hinge specialization (see asterisk in Fig. 9*A*). The loss of umbrella cells and disruption of cell-cell interactions are consistent with the decreases in TER and the large increases in urea permeability observed in cats with FIC. These findings also were consistent

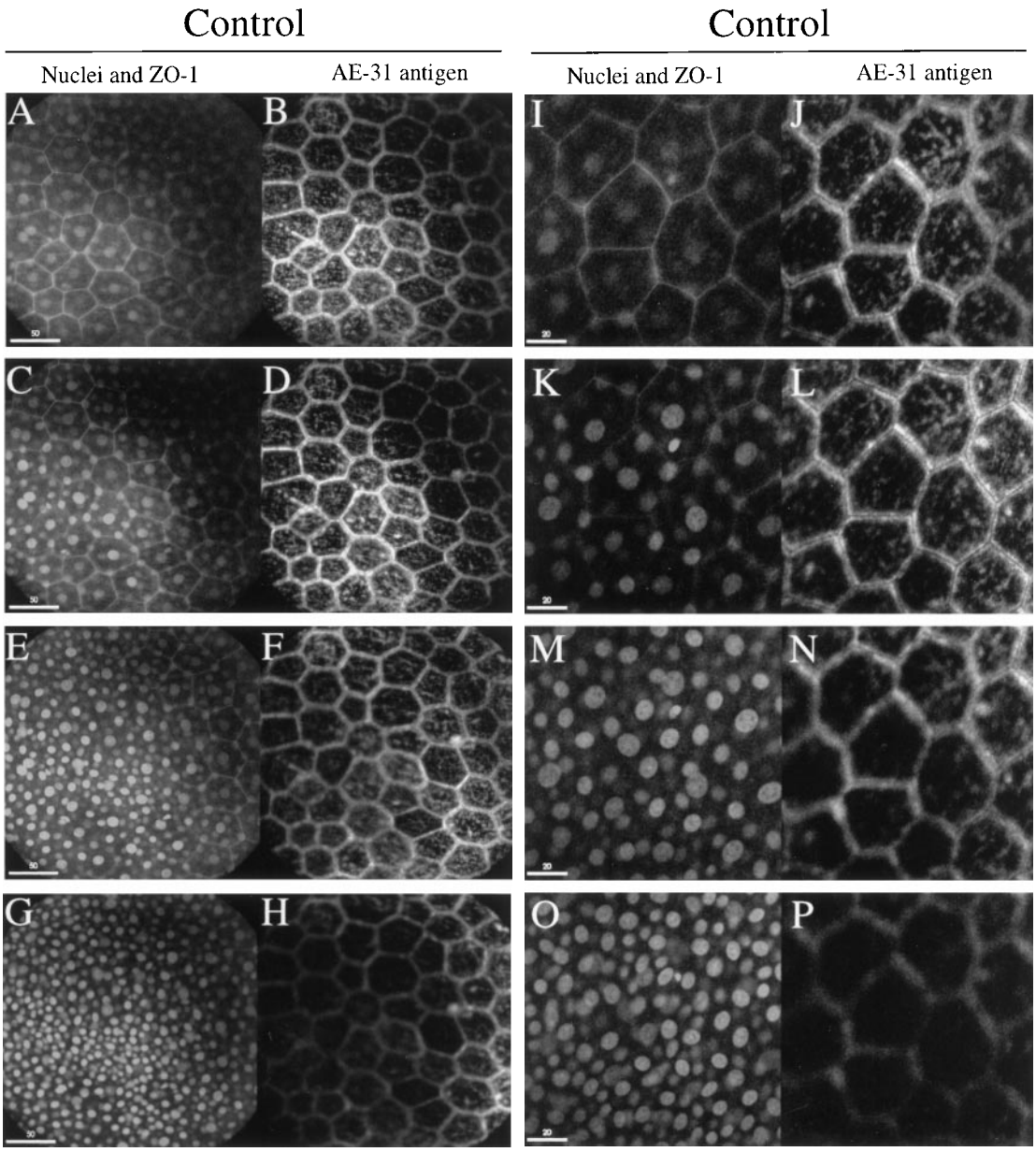

Fig. 6. Scanning laser confocal microscopy of undistended bladder urothelium from control cats. Dissected urothelium was fixed with paraformaldehyde and stained for AE-31 antigen, for tight junction protein ZO-1, and for nucleus. Low-magnification overviews are shown in *A–H*, and higher magnification images are shown in *I–P*. Individual optical sections, obtained with a scanning laser confocal microscope, are shown from the apical pole of umbrella cells at or above the level of the tight junctions (*A*, *B*, *I*, and *J*), 2–3 μm below this level (*C*, *D*, *K*, and *L*), 2–3 μm below the previous section (*E*, *F*, *M*, and *N*), and 2–3 μm below the previous section (*G*, *H*, *O*, and *P*). Samples were scanned simultaneously for FITC (for AE-31 antigen, *right*) and Texas Red (ZO-1 and nuclei, *left*) (or propidium iodide) emission. Note that the epithelial cell layer in *A–H* is not perfectly flat so that cells in the *top right* of these panels are lower than those in the *bottom left* half of the image.

with the findings of confocal immunofluorescence microscopy.

The bladders of two normal cats and four cats with FIC were examined by scanning electron microscopy after hydrodistention. In both normal bladders the urothelium appeared similar to that observed in undistended tissue (Fig. 10, *A* and *B*). Multiple changes were observed in distended bladders from animals with FIC. In some samples large regions of umbrella cells were missing and the underlying intermediate cell layer was observed (Fig. 10, *C* and *D*). The surface of many of the umbrella cells in these regions looked relatively smooth (i.e., lacked the characteristic angular folds observed in control cells) or showed a patchy morphology in which smooth regions were interspersed with regions that contained plaque/hinges (Fig. 10*D*). In several of the samples, large regions of the epithelium (including umbrella, intermediate, and basal cell layers) were found denuded and the underlying connective tissue could then be observed (Fig. 10, *E* and *F*). In one of the

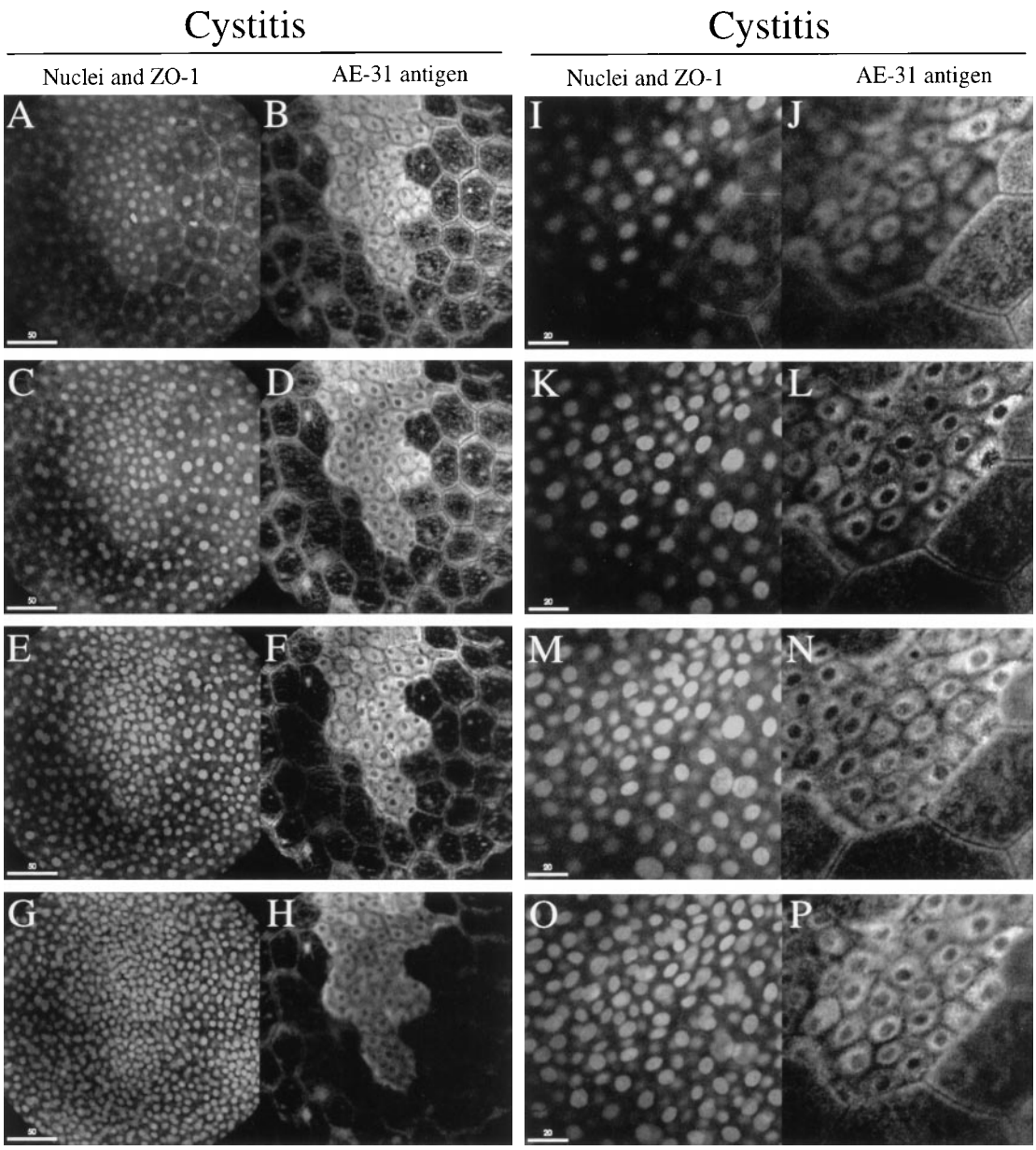

Fig. 7. Scanning laser confocal microscopy of undistended bladder urothelium from FIC cats. Dissected urothelium was fixed with paraformaldehyde and stained for AE-31 antigen, for tight junction protein ZO-1, and for nucleus. Low-magnification overviews are shown in *A–H*, and higher magnification images are shown in *I–P*. Individual optical sections, obtained with a scanning laser confocal microscope, are shown from the apical pole of umbrella cells at or above the level of the tight junctions (*A*, *B*, *I*, and *J*), 2–3 μm below this level (*C*, *D*, *K*, and *L*), 2–3 μm below the previous section (*E*, *F*, *M*, and *N*), and 2–3 μm below the previous section (*G*, *H*, *O*, and *P*). Samples were scanned simultaneously for FITC (*right*) and Texas Red (*left*) (or propidium iodide) emission.

samples, the epithelium looked fairly normal, possibly representing an animal in which only a mild case of FIC was present. This is consistent with the occasional FIC bladder that had high TER and low permeabilities to water and urea and with previous in vivo studies (15). Where the umbrella cells are denuded, the adjacent cells look somewhat flattened, possibly in an attempt to close or repair the defect.

Transmission electron microscopy. Transmission electron microscopy was employed to provide high-resolution views of the urothelium in cross section. The samples were taken at the same time as those for scanning electron microscopy. Transmission electron micrographs of normal undistended cat bladders revealed several features typical for umbrella cells (see Fig. 11, *A* and *B*). These include highly developed tight junctions (Fig. 11*B*), asymmetric unit membranes containing plaques and "hinge regions" on the apical surface (Fig. 11*A*) and numerous subapical membrane vesicles with an appearance similar to that of the apical membrane (Fig. 11*B*).

In cats with FIC, tight junctions had come apart, leading to disruption of the epithelial layer. In areas where the epithelium was not denuded, the ultrastructure of the cells appeared normal, with the characteristic apical surface and subapical vesicles. It was possible

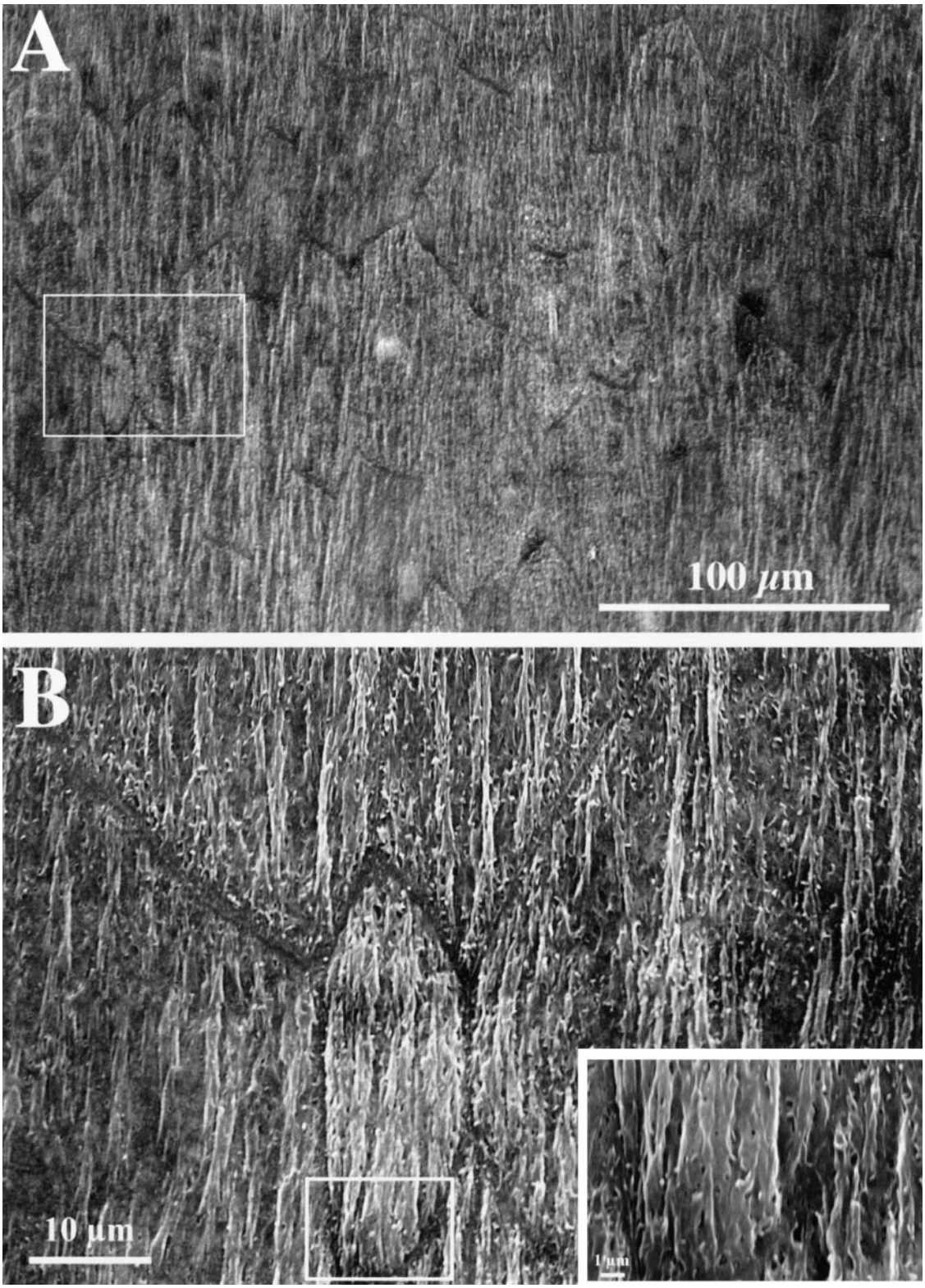

Fig. 8. Scanning electron microscopy (SEM) analysis of undistended bladders from normal cats. *A*: low-magnification overview of bladder epithelium. *B*: close-up of individual umbrella cells enclosed by box in *A*. *Inset* in *B* is of box in *B*.

to find umbrella cells with disrupted tight junctions that exhibited normal apical membrane and subapical vesicle structure (data not shown).

In other areas, the umbrella cell layer had an electron lucent appearance, lacked normal cytoplasmic density, and discontinuities in the apical plasma membrane were observed (Fig. 11*C*). Cells with this morphology lacked clear plaque/hinge regions and there was a paucity of subapical vesicles. In other regions, areas where umbrella cells were denuded from the underly-

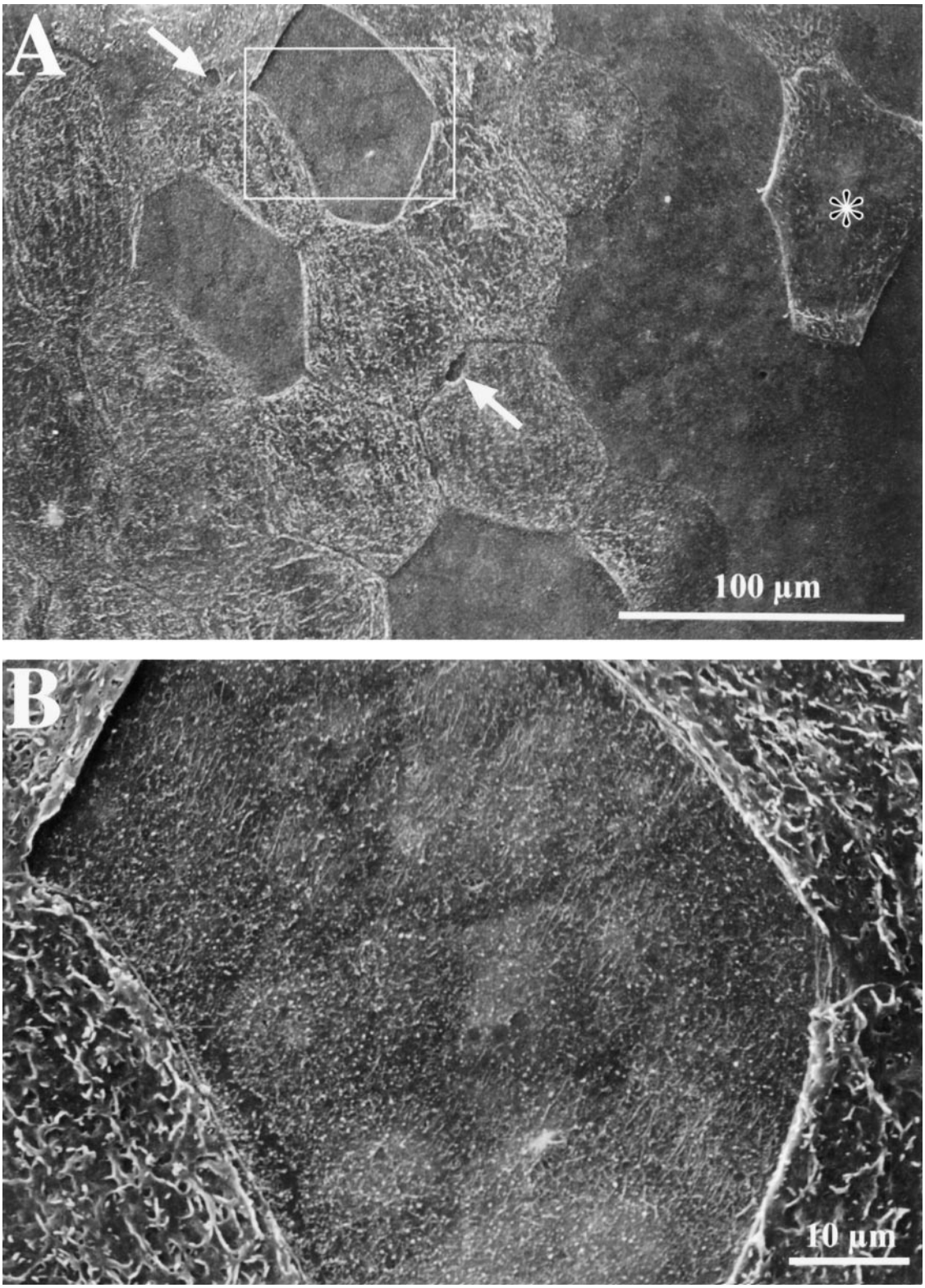

Fig. 9. SEM analysis of undistended bladders from FIC cats. *A*: low-magnification overview of bladder epithelium. Arrows show regions where cell-cell interactions between adjacent umbrella cells are disrupted. Apical surface of cell marked with an asterisk is relatively smooth and lacks hinge regions. *B*: close-up of area enclosed by box in *A*. Underlying intermediate cells are discernible.

ing cell layers were observed. In Fig. 11*D*, we show a region at the edge of one of these denuded areas where a piece of umbrella cell is seen attached to an adjacent cell (note the aberrant tight junction at the *left* of Fig. 11*D*). The region to the *left* of this cell lacked an umbrella cell layer. Finally, in regions where the umbrella cell layer was disrupted, the underlying intermediate and basal cell layers often appeared vacuolated

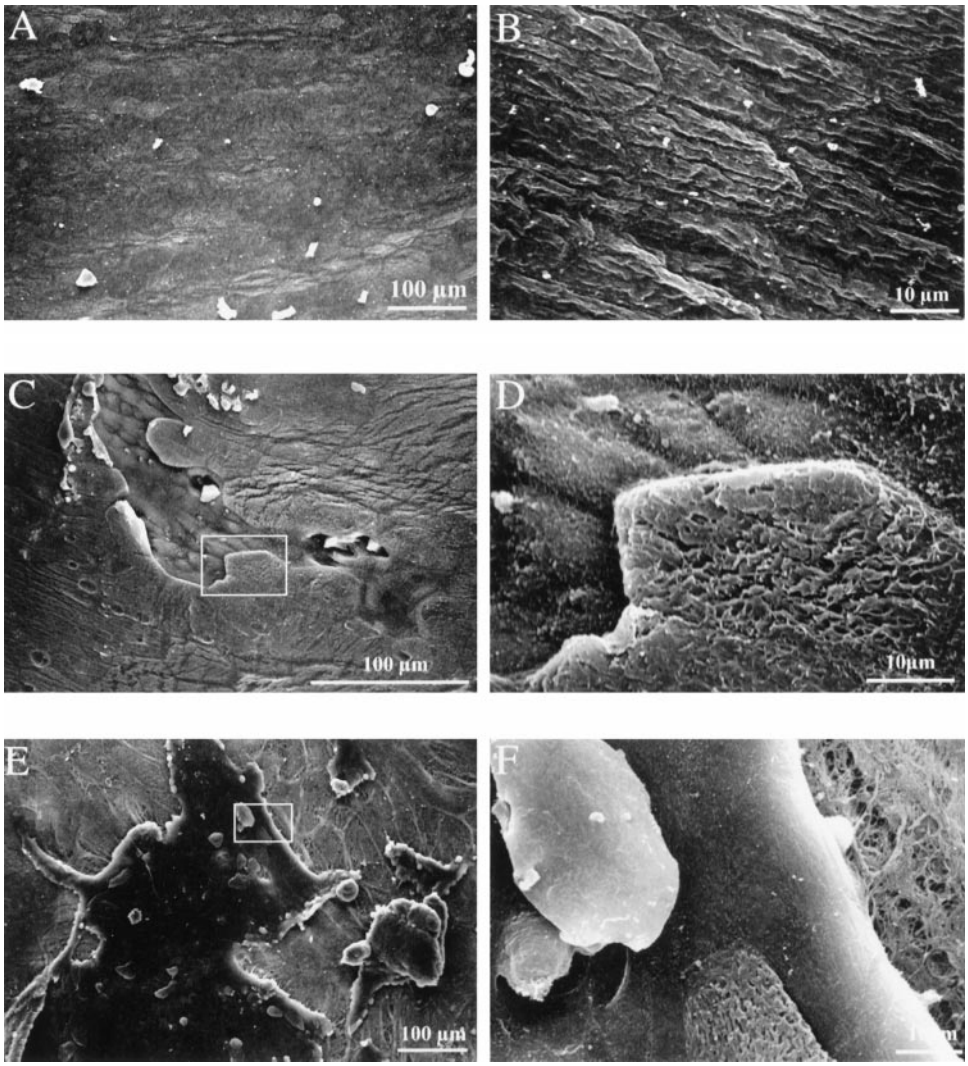

Fig. 10. SEM analysis of hydrodistended bladders from normal and FIC cats. *A*: low-magnification view of control bladder. *B*: high-magnification view of control bladder showing individual umbrella cells. *C*: low-magnification view of FIC bladder demonstrating region where umbrella cell layer is disrupted. *D*: close-up of area enclosed by box in *C*. *E*: low-magnification view of FIC bladder showing regions where the urothelium is denuded from the underlying connective tissue. *F*: close-up of area enclosed by box in *E*.

and had a stellate or bloated appearance (data not shown).

DISCUSSION

To maintain normal plasma composition and volume homeostasis, the kidney excretes urine, which is very different in composition from the plasma. Urine osmolalities vary from 50 to 1,000 mosmol/kg, with pH values as low as 4.5, and concentrations of urea, ammonium, and potassium that are severalfold higher than those of the plasma.

The bladder stores the urine for considerable periods, expanding its surface area as urine accumulates. It is clear that the ability of the kidney to perform its function requires that the bladder prevent leakage of urine constituents into the blood. To achieve this barrier function, the umbrella cells maintain apical membranes of exceptionally low permeability and tight junctions, which can maintain extraordinarily high resistances (9, 25). As the bladder fills, it is hypothesized that large numbers of submembrane vesicles containing apical membrane proteins such as uroplakins and AE-31 fuse with the surface, expanding the surface area of each umbrella cell. Voiding results in a wave of endocytosis, restoring the smaller surface areas of the umbrella cells (9, 18, 19, 26, 29, 41).

Failure of barrier function would clearly compromise homeostasis. However, the bladder wall is richly supplied with nociceptor C-type afferent nerve fibers, which terminate just under the urothelium and the bladder wall smooth muscle (28), and are sensitive to many urine constituents, such as high potassium (38). Accordingly, when the bladder permeability barrier fails, it is believed that a chemical stimulation of the nociceptor afferents and irritation of the detrusor muscle provoke frequency, urgency, nocturia, and bladder pain, which are the hallmarks of cystitis (3, 4). When these symptoms occur, the frequent voiding reduces the contact time of the urine with the bladder so that leakage across the barrier is diminished. The tendency of cystitis sufferers to drink additional fluid reduces the concentration gradients in the urine, thus reducing the chemical potential for leakage. However, no direct proof of a neuroepithelial interaction has been demonstrated to date.

In bacterial or toxin-induced (e.g., cyclophosphamide) cystitis, agents such as acrolein (24) or hemolysin (30) injure the urothelium, leading to symptoms. For

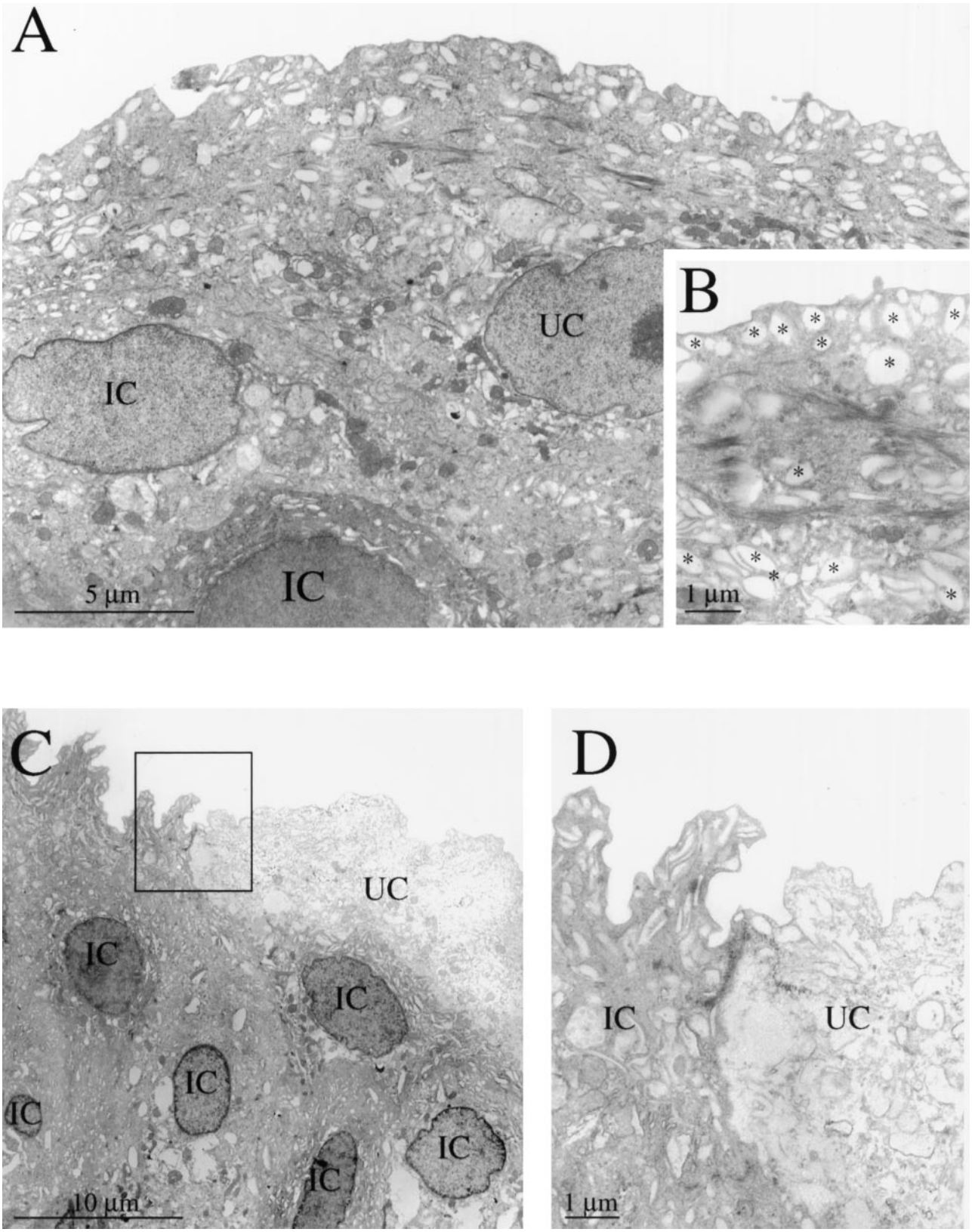

Fig. 11. Transmission electron microscopy analysis of undistended bladders from normal and FIC cats. *A*: low-power view of normal umbrella cell (UC). *B*: high-magnification view of subapical endosomes (*). *C* and *D*: cross sections through urothelium of FIC cats. Umbrella cell has lost cytoplasmic structure (*C*) and is necrotic, and intermediate cell (IC) is now in apical (luminal) position with formation of subapical endosomes (*D*). *D*: close-up of area enclosed by box in *C*.

patients with IC, the causative agent is unknown, but the symptoms are the same, and they persist because the cause(s) is not reversed. In the case of IC, numerous studies have failed to identify a causative agent. The fact that similar forms of cystitis without an apparent cause occur also in cats and other mammals suggests that the mammalian bladder is prone to some form of as-yet-undefined injury, at least in several species.

Because of the lack of a well-characterized animal model, the mechanisms involved in the onset and symptomatology of IC have not been defined, and treatment is empiric. Early findings, suggesting that damage to the urothelial glycosaminoglycan (GAG) layer might be involved in IC, have led urologists to try treatments of heparin, hyaluronic acid, and pentosanpolysulfate, in an effort to repair the GAG layer (31, 35). Because of evidence for increased mast cell density and activation in the bladder walls of IC patients, antihistamines have been tried as well (40). Finally, for its "anti-inflammatory" properties, DMSO has been administered via bladder catheter (34, 39). Although controlled trials of these therapies are rare, at best they appear to offer only limited benefit to patients. Clearly, studies of etiology and therapeutics of IC need an animal model of the disease. The present studies were performed to define in detail the functional and structural effects of FIC on cat urothelium. Most of the studies presented here uniquely demonstrate both structural and permeability properties of the same bladder.

It has been suggested that FIC may not represent an adequate model of IC (11); however, this suggestion is based on early research into cystitis in cats when the definition of FIC had not been fully elucidated. More recently, better comparisons between FIC and IC have been systematically made, thus suggesting that although the precise etiology of both FIC and IC remain undefined, FIC provides a good model for IC at the current time (8).

Like human IC, FIC occurs in cats of varying ages, appears spontaneously, and may remit. The symptoms appear similar to the human syndrome and, like the human disease, can be extremely debilitating, so that FIC is a leading reason for euthanizing pet cats. Both IC and FIC can manifest with Hunner's ulcers on cystoscopy. The only major difference between IC and FIC is the nine to one preponderance of females in IC and the equal sex distribution in FIC. However, recent data suggest that some forms of chronic prostatitis found in males may actually be IC (2).

The data obtained on control undistended and hydrodistended bladders agree with results we and others have previously obtained in rabbit, rat, mouse, and guinea pig, indicating that the bladders of all of these species, and likely that of the human, exhibit striking barrier function. The ultrastructural and fluorescence microscopy data on control bladders agree with careful prior descriptions in multiple species (12, 20, 29, 41), including our own findings in guinea pigs (23). Features shared with other species, including human urothelium, include well-developed tight junctions, asymmetric unit membranes with rigid-appearing plaques and bent "hinge" areas, and abundant subapical vesicles that feature membranes resembling the asymmetric unit membrane of the apical surface. We believe that the permeability of the human urothelial apical membrane is also low, but to date we have not been able to measure it.

Our studies in bladders from FIC cats have demonstrated a clear-cut failure of the bladder permeability barrier in affected cats, with increased leakage of ions across the epithelium (reduced TER) and urea leakage in nonhydrodistended bladders. Following hydrodistention, urothelia from cats affected with FIC exhibited marked increases in both urea and water permeabilities. These results demonstrate that the urothelium in FIC bladders leaks under basal conditions and that the leakage worsens when the bladder must accommodate increasing amounts of urine, suggesting that the tissue has lost the ability to add low permeability urothelial surface area.

The structural studies demonstrate patches that are devoid of umbrella cells in FIC bladders. Transmission electron microscopy reveals detachment of umbrella cells from each other, with disruption of tight junctions. We have obtained similar findings in an autoimmune model of cystitis involving acute inflammation of sensitized guinea pigs to ovalbumin instilled within the bladder lumen (23). In this model, massive acute inflammation and edema of the bladder wall accompanied epithelial cell damage. No such edema or inflammation was observed in the cats with FIC. These results demonstrate direct epithelial damage in FIC and, by extension, IC, and raise the possibility that the epithelial damage, possibly to the tight junction first, represents the inciting lesion in these disorders. Transmission electron microscopy of the human bladder in IC demonstrates similar results with widened tight junctions and loss of apical cells (12). Whether these findings in the human are exactly the same as in the cat is unknown.

Given the fact that the permeability barrier is composed of the apical membranes of umbrella cells and the tight junctions between the cells, it may seem surprising that FIC bladders exhibited any resistance or permeability barrier at all. Of course, with any disease process, the extent of involvement may vary, and varying proportions of the tissue were likely denuded in differing Ussing chamber experiments. In this regard, comparison of TER and urea permeability in Fig. 6 shows that the leakier the bladder was to ions (lower TER), the leakier it was as well to urea (higher urea permeability). These results suggest that areas which were denuded of umbrella cells may have caused increased leakiness to both urea and ions.

The structural studies also reveal evidence for differentiation of underlying urothelial cells in FIC bladders, in that they expressed AE-31 but not ZO-1. These results raise the possibility that these underlying cells may be differentiating toward becoming umbrella cells. The extent to which such cells may contribute to barrier function remains unclear, but these cells, unlike under-

lying urothelial cells in normal bladder, may represent a barrier to ion, neutral solute, and water fluxes.

In the FIC animals, we noted also a small increase in the TER in the distended state compared with the empty bladders. Although this result was not significant, it suggests the possibility that the process of increased surface apical membrane in the normal parts of the urothelium in response to distension may still be continuing. However, because of the damage to the rest of the urothelium, the effect is not marked. Conceptually it would be expected for the TER to decrease with increased permeability; however, as outlined above, this does not happen in the FIC distended bladders. The exact relationship between TER and permeability is unclear. The TER is a function of ion transport across the membrane, and clearly, if the membrane has denuded areas or holes, then the ion transport is greatly increased. Urea and water diffusion across the membrane should follow the pattern of the ion flux, particularly if the reason for the increased ion flux is the partially damaged membrane. The ion fluxes across the membrane, though, are independent of the urea and water diffusion, as there are amiloride-sensitive sodium channels on the apical membrane of the urothelium as well as paracellular pathways. In MDCK cells, the decrease in TER due to holes being made in the monolayer does not correlate directly with the loss of surface area from these holes (14).

Taken together, these results demonstrate direct epithelial damage and failure of barrier function in an animal model of IC. They suggest that IC may be caused by just such an epithelial lesion, with resulting irritation, symptoms, and inflammation arising from the noxious effect of urine constituents on the underlying bladder wall layers. Further studies in animal models are needed to test this hypothesis by inducing direct and selective epithelial injury and defining the effects of leakage of urine constituents on the underlying bladder wall. Since there is some evidence for failure of barrier function and epithelial damage in human IC, our results link this animal model more closely with the human disease, opening the way for detailed studies of etiology and potential therapies in these animals. Development of models of selective umbrella cell damage will permit studies designed to develop special diets to reduce the content of noxious irritants in the urine; such diets may help ease the symptoms in IC patients.

This work was supported in part by National Institute of Diabetes and Digestive and Kidney Diseases Grants R-37-DK-48217–05 (to M. L. Zeidel), R-01-DK-54425–01 (to G. Apodaca), and RO-1-DK-47538 (to C. A. T. Buffington). This work was supported in part by a grant from the AFUD/AUA Research Scholar Program and The National Bladder Foundation.

Address for reprint requests and other correspondence: M. L. Zeidel, Dept. of Medicine, 1218 Scaife Hall, 3550 Terrace St., Pittsburgh, PA 15261 (E-mail: zeidel@msx.dept-med.pitt.edu).

Received 23 March 1999; accepted in final form 27 October 1999.

REFERENCES

1. **Apodaca G, Katz LA, and Mostov KE.** Receptor-mediated transcytosis of IgA in MDCK cells is via apical recycling endosomes. *J Cell Biol* 125: 67–86, 1994.
2. **Berger RE, Miller JE, Rothman I, Krieger JN, and Muller CH.** Bladder petechiae after cystoscopy and hydrodistension in men diagnosed with prostate pain. *J Urol* 159: 83–85, 1998.
3. **Birder LA and de Groat WC.** Increased c-fos expression in spinal neurons after irritation of the lower urinary tract in the rat. *J Neurosci* 12: 4878–4889, 1992.
4. **Birder LA and de Groat WC.** Induction of c-fos expression in spinal neurons by nociceptive and nonnociceptive stimulation of LUT. *Am J Physiol Regulatory Integrative Comp Physiol* 265: R326–R333, 1993.
5. **Bomsel M, Prydz K, Parton RG, Gruenberg J, and Simons K.** Endocytosis in filter-grown Madin-Darby canine kidney cells. *J Cell Biol* 109: 3243–3258, 1989.
6. **Buffington CA.** Lower urinary tract disease in cats: new problems new paradigms. *J Nutr* 124: 2643S–2651S, 1994.
7. **Buffington CA, Blaisdell JL, Binns SPJ, and Woodworth BE.** Decreased urine glycosaminoglycan excretion in cats with interstitial cystitis. *J Urol* 155: 1801–1804, 1996.
8. **Buffington CA, Chew DJ, and DiBartola SP.** Interstitial cystitis in cats. *Vet Clin North Am Small Anim Pract* 26: 317–326, 1996.
9. **Chang A, Hammond TG, Sun TT, and Zeidel ML.** Permeability properties of the mammalian bladder apical membrane. *Am J Physiol Cell Physiol* 267: C1483–C1492, 1994.
10. **Dixon JS, Holm-Bentzen M, Gilpin CJ, Gosling JA, Bostofte E, Hald T, and Larsen S.** Electron microscopic investigation of the bladder urothelium and glycocalyx in patients with interstitial cystitis. *J Urol* 135: 621–625, 1986.
11. **Elbadawi A.** Interstitial cystitis: a critique of current concepts with a new proposal for pathologic diagnosis and pathogenesis. *Urology* 49: 14–40, 1997.
12. **Elbadawi AE and Light JK.** Distinctive ultrastructural pathology of nonulcerative interstitial cystitis: new observations and their potential significance in pathogenesis. *Urol Int* 56: 137–162, 1996.
13. **Fall M, Johansson SL, and Aldenborg F.** Chronic interstitial cystitis: a heterogeneous syndrome. *J Urol* 137: 35–38, 1987.
14. **Fuller SD and Simons K.** Transferrin receptor polarity and recycling accuracy in "tight" and "leaky" strains of Madin-Darby canine kidney cells. *J Cell Biol* 103: 1767–1779, 1986.
15. **Gao X, Buffington CA, and Au JL.** Effect of interstitial cystitis on drug absorption from urinary bladder. *J Pharmacol Exp Ther* 271: 818–823, 1994.
16. **Gunning ME, Ballermann BJ, Silva P, Brenner BM, and Zeidel ML.** Characterization of ANP receptors in rabbit inner medullary collecting duct cells. *Am J Physiol Renal Fluid Electrolyte Physiol* 255: F324–F330, 1988.
17. **Hicks RM.** The permeability of rat transitional epithelium. Kertinization and the barrier to water. *J Cell Biol* 28: 21–31, 1966.
18. **Hicks RM.** The mammalian urinary bladder: an accommodating organ. *Biol Rev Camb Philos Soc* 50: 215–246, 1975.
19. **Hicks RM, Ketterer B, and Warren RC.** The ultrastructure and chemistry of the luminal plasma membrane of the mammalian urinary bladder: a structure with low permeability to water and ions. *Philos Trans R Soc Lond B Biol Sci* 268: 23–38, 1974.
20. **Jost SP, Gosling JA, and Dixon JS.** The morphology of normal human bladder urothelium. *J Anat* 167: 103–115, 1989.
21. **Kikeri D, Sun A, Zeidel ML, and Hebert SC.** Cell membranes impermeable to NH3. *Nature* 339: 478–480, 1989.
22. **Kikeri D, Sun A, Zeidel ML, and Hebert SC.** Cellular NH_4^+/K^+ transport pathways in mouse medullary thick limb of Henle. Regulation by intracellular pH. *J Gen Physiol* 99: 435–461, 1992.
23. **Lavelle JP, Apodaca G, Meyers SA, Ruiz WG, and Zeidel ML.** Disruption of guinea pig urinary bladder permeability barrier in noninfectious cystitis. *Am J Physiol Renal Physiol* 274: F205–F214, 1998.
24. **Levine LA and Richie JP.** Urological complications of cyclophosphamide. *J Urol* 141: 1063–1069, 1989.
25. **Lewis SA, Berg JR, and Kleine TJ.** Modulation of epithelial permeability by extracellular macromolecules. *Physiol Rev* 75: 561–589, 1995.

26. **Lewis SA and de Moura JL.** Incorporation of cytoplasmic vesicles into apical membrane of mammalian urinary bladder epithelium. *Nature* 297: 685–688, 1982.
27. **Lewis SA and Hanrahan JW.** Physiological approaches for studying mammalian urinary bladder epithelium. *Methods Enzymol* 192: 632–650, 1990.
28. **Maggi A.** The dual function of capsaicin-sensitive sensory nerves in the bladder and urethra C. *Ciba Found Symp* 151: 77–83, 1990.
29. **Minsky BD and Chlapowski FJ.** Morphometric analysis of the translocation of lumenal membrane between cytoplasm and cell surface of transitional epithelial cells during the expansion-contraction cycles of mammalian urinary bladder. *J Cell Biol* 77: 685–697, 1978.
30. **Mobley HL, Chippendale GR, Tenney JH, Hull RA, Warren, and JW.** Expression of type 1 fimbriae may be required for persistence of *Escherichia coli* in the catheterized urinary tract. *J Clin Microbiol* 25: 2253–2257, 1987.
31. **Morales A, Emerson L, Nickel JC, and Lundie M.** Intravesical hyaluronic acid in the treatment of refractory interstitial cystitis. *J Urol* 156: 45–48, 1996.
32. **Negrete HO, Lavelle JP, Berg J, Lewis SA, and Zeidel ML.** Permeability properties of the intact mammalian bladder epithelium. *Am J Physiol Renal Fluid Electrolyte Physiol* 271: F886–F894, 1996.
33. **O'Guin WM, Sun TT, and Manabe M.** Interaction of trichohyalin with intermediate filaments: three immunologically defined stages of trichohyalin maturation. *J Invest Dermatol* 98: 24–32, 1992.
34. **Parkin J, Shea C, and Sant GR.** Intravesical dimethyl sulfoxide (DMSO) for interstitial cystitis: a practical approach. *Urology* 49: 105–107, 1997.
35. **Parsons L.** Epithelial coating techniques in the treatment of interstitial cystitis C. *Urology* 49: 100–104, 1997.
36. **Parsons CL, Boychuk D, Jones S, Hurst R, and Callahan H.** Bladder surface glycosaminoglycans: an epithelial permeability barrier. *J Urol* 143: 139–142, 1990.
37. **Parsons CL, Lilly JD, and Stein P.** Epithelial dysfunction in nonbacterial cystitis (interstitial cystitis). *J Urol* 145: 732–735, 1991.
38. **Parsons CL, Stein PC, Bidair M, and Lebow D.** Abnormal sensitivity to intravesical potassium in interstitial cystitis and radiation cystitis. *Neurourol Urodyn* 13: 515–520, 1994.
39. **Sant GR.** Intravesical 50% dimethyl sulfoxide (Rimso-50) in treatment of interstitial cystitis. *Urology* 29: 17–21, 1987.
40. **Seshadri P, Emerson L, and Morales A.** Cimetidine in the treatment of interstitial cystitis. *Urology* 44: 614–616, 1994.
41. **Staehelin LA, Chlapowski FJ, and Bonneville MA.** Lumenal plasma membrane of the urinary bladder. I. Three-dimensional reconstruction from freeze-etch images. *J Cell Biol* 53: 73–91, 1972.
42. **Yu J, Lin JH, Wu XR, and Sun TT.** Uroplakins Ia and Ib, two major differentiation products of bladder epithelium, belong to a family of four transmembrane domain (4TM) proteins. *J Cell Biol* 125: 171–182, 1994.
43. **Yu J, Manabe M, and Sun TT.** Identification of an 85–100 kDa glycoprotein as a cell surface marker for an advanced stage of urothelial differentiation: association with the inter-plaque ("hinge") area. *Epithelial Cell Biol* 1: 4–12, 1992.
44. **Yu J, Manabe M, Wu XR, Xu C, Surya B, and Sun TT.** Uroplakin I: a 27-kD protein associated with the asymmetric unit membrane of mammalian urothelium. *J Cell Biol* 111: 1207–1216, 1990.
45. **Zeidel L.** Low permeabilities of apical membranes of barrier epithelia: what makes watertight membranes watertight? *Am J Physiol Renal Fluid Electrolyte Physiol* 271: F243–F245, 1996.